Anisotropic thermal transport in highly ordered TiO_2 nanotube arrays

Liying Guo,[1] Jun Wang,[2] Zhiqun Lin,[2] Sobieslaw Gacek,[1] and Xinwei Wang[1,a)]
[1]*Department of Mechanical Engineering, 2010 Black Engineering Building, Iowa State University, Ames, Iowa 50011, USA*
[2]*Department of Materials Science and Engineering, Iowa State University, Ames, Iowa 50011, USA*

(Received 28 June 2009; accepted 14 November 2009; published online 28 December 2009)

This paper reports on the anisotropic thermal transport in highly ordered amorphous and anatase TiO_2 nanotube arrays. Strong anisotropic thermal conductivity is observed: 0.617 W K^{-1} m^{-1} along the tube length direction and 0.077–0.102 W K^{-1} m^{-1} in the cross-tube direction for amorphous TiO_2 nanotube arrays. The anatase TiO_2 nanotube arrays are found to have a higher and anisotropic thermal conductivity, 1.12 W K^{-1} m^{-1} in the tube-length direction and 0.24 W K^{-1} m^{-1} in the cross-tube direction. The experimental results show that the density of the nanotube arrays is much lower than the value estimated from the geometry of the nanotube array, largely due to the existence of defects and loose contact among nanotubes. The thermal contact resistance between TiO_2 nanotubes is characterized to be 15.1 and 20.6 K m^2 W^{-1} for the two measured amorphous samples, and 5.90 K m^2 W^{-1} for the anatase TiO_2 nanotubes. This quantitatively proves that annealing of amorphous TiO_2 nanotubes to transform them to anatase phase also improves the contact between nanotubes. © *2009 American Institute of Physics*. [doi:10.1063/1.3273361]

I. INTRODUCTION

In recent years, TiO_2 has attracted increasing interest as an environmental cleaning ceramic material and has been fabricated into nanostructures, such as nanoparticles, thin films, and nanofibers. Highly ordered, vertically oriented, freestanding TiO_2 nanotube arrays fabricated by anodization have received considerable attention due to its unique structure of high surface-to-volume and length-to-diameter ratios. Three generations of techniques have been developed in the past to produce TiO_2 nanotube arrays.[1] Studies were also carried out on the fabrication of TiO_2 nanotube arrays on different substrates to suite varied applications.[1–3] These techniques have enabled the production of TiO_2 nanotube arrays with various pore to pore distance, diameter, and wall thickness through controlling the water content, *p*H value, voltage, and temperature.[1,3,4] TiO_2 nanotube arrays with length from several hundred nanometers to 1 mm have been fabricated successfully.[5] Owing to their narrower band gap and remarkable architecture, TiO_2 nanotubes have the great potential to control the lateral spacing geometry and regulate cell fate,[3] to utilize visible light energy, to enhance electron transport and suppress recombination, and to provide large sensing and reacting areas.[6–8] To date, TiO_2 nanotubes have been applied to various areas including biomedical implant devices,[3] biomedical diagnostic applications, gas sensors, solar cells, fuel cells, lean-burn gasoline engines, and photocatalyst.[9–14]

Concerns have arisen about severe thermal issues in fabricating and functioning of TiO_2 nanotube arrays due to extremely localized electrical, optical, and mechanical heating. Different thermal response of the base material and TiO_2 nanotube arrays could lead to material interface sliding, structure degrading, efficiency downgrading, and mechanical failure. To predict, evaluate, and improve the thermal performance of TiO_2 nanotube arrays during their fabrication and engineering applications, solid experimental data about the thermophysical properties of such nanostructures becomes extremely important. Thermal properties of a material down to micro/nanoscale can be dramatically different from those of the bulk counterpart.[15] In the past, little work has been done with respect to the thermal management in the applications of TiO_2 nanotube arrays. In this work, we report the experimental characterization of anisotropic thermophysical properties of highly ordered TiO_2 nanotube arrays and pioneer the evaluation of thermal contact resistance between TiO_2 nanotubes by using our recently developed transient-electrothermal (TET) technique[16] and photothermal (PT) method.[17] The TiO_2 nanotubes in the measured samples have an average inner diameter, center-to-center distance, and wall thickness of 90, 120, and 15 nm, respectively.

II. EXPERIMENTAL DETAILS

A. Sample preparation

In this work, highly ordered TiO_2 nanotube arrays are grown on a Ti foil using a modified procedure.[1,18,19] Briefly, Ti foil (Sigma-Aldrich; 250 μm thick, 99% purity) is first degreased by ultrasonication for 30 min in a mixture of acetone, methanol, and methylene chloride, followed by a thorough rinse with de-ionized (DI) water and blow drying with N_2 gas. Ethylene glycol (Fisher Scientific) is used as the electrolyte. A small amount of ammonium fluoride (Sigma-Aldrich) is added into the ethylene glycol electrolyte. All chemicals and materials in the experiment are used as received without further purification. Electrochemical anodization of Ti foil is carried out in a two-electrode cell at room temperature using a power source EC570-90 (Thermo Electron Corporation), in which a platinum foil is used as the

a)Author to whom correspondence should be addressed. Electronic mail: xwang3@iastate.edu. Tel.: (515) 294-2085. FAX: (515) 294-3261.

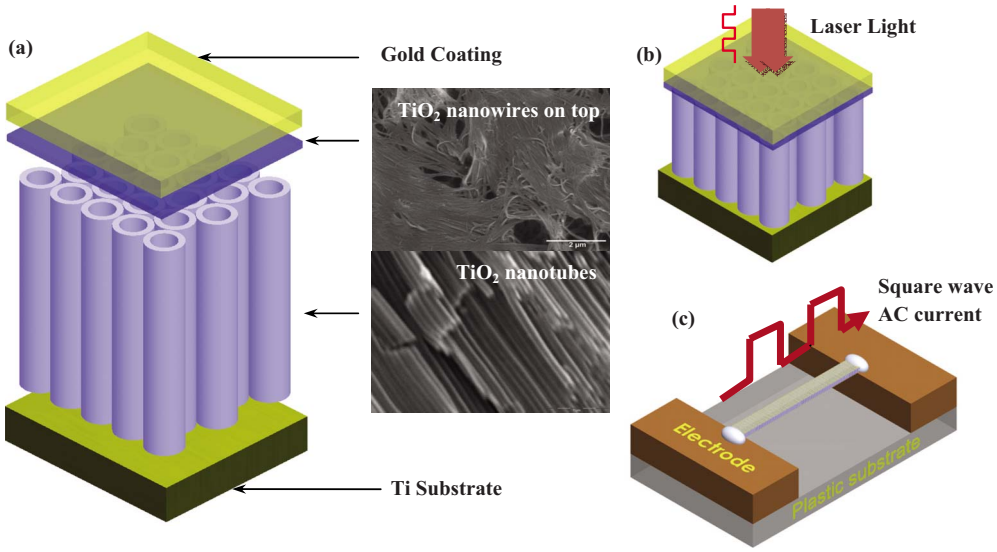

FIG. 1. (Color online) Schematic structure of the TiO_2 nanotube arrays. (a) General structure for TiO_2 nanotubes fabricated on Ti substrate. From top to bottom, the layers are gold coating, TiO_2 nanowires, TiO_2 nanotubes, and Ti substrate; (b) sample 1 for the PT experiment; (c) freestanding TiO_2 nanotube arrays sample for TET experiment. The figures are not to scale.

counterelectrode. Anodization is conducted at a constant potential of 60 V for a period of time until a desired thickness is reached. After anodization the Ti foil with the TiO_2 nanotubes is thoroughly washed with a large amount of DI water and methanol, and dried by N_2 gas flow. As-prepared TiO_2 nanotube arrays were amorphous and can be readily transformed into anatase crystalline by annealing in air at 500 °C for 3 h.[1,18,20] The anatase formation was confirmed by Raman spectroscopy and was detailed in our previous work.[20] It is noteworthy that no change on the nanotubular morphology after high temperature annealing was observed according to the scanning electron microscopy (SEM) characterization. As-prepared TiO_2 nanotube arrays are covered by a thin layer of TiO_2 nanowires,[1,18] which prevent the sputtering deposited gold from penetrating into the nanotube channels. In this work, samples 1 and 3 are obtained after anodization for 4 h Sample 2 is obtained after anodization for 60 h. To characterize the thermal transport phenomena in amorphous nanotube arrays, sample 1 and two small pieces cut off sample 2 are used and coated with a thin gold layer of about 200 nm. Sample 3 and the leftover of sample 2 [sample 2(c)] are annealed at 500 °C for 3 h to obtain anatase crystalline and coated with a thin gold layer of 200 nm for sample 3 and 150 nm for sample 2(c). This gold coating layer is used in the PT experiment to absorb the laser energy, and is used as the heater and thermal sensor in the TET experiment as detailed below.

Figure 1(a) shows the schematic structure of the sample. From the top to bottom, the layers shown are gold coating, TiO_2 nanowires, free TiO_2 nanotubes, and Ti substrate. The TiO_2 nanotubes are fabricated on a Ti substrate. For the TET measurement, the TiO_2 nanotube arrays are taken off the Ti substrate to make them freestanding. For the sample measured using the PT technique, the thickness of these layers are 200 or 150 nm, 100 nm, 29.2 μm (for amorphous) and 30.7 μm (for anatase), and 250 μm, respectively.

B. Thermal characterization

Using the amorphous TiO_2 nanotube arrays as an example, we give the details of thermal characterization. First of all, the density (ρ_{eff}) and thermal conductivity ($k_{\parallel}$) of the amorphous TiO_2 nanotube arrays (sample 1) are characterized along the tube direction using the PT technique. Sample 2 (140 μm thick) is too thick for the PT experiment. Therefore, sample 1 is used to study the heat transfer along the tube axial direction. For studying the heat transfer in the cross-tube direction using the TET technique, freestanding TiO_2 nanotube array from sample 1 is too thin and easily breaks when it is suspended between electrodes. Therefore, sample 2 is used for studying the heat transfer in the cross-tube direction. These two samples are fabricated using the same technique under the exact same experimental conditions. Therefore, they are expected to have the same thermophysical properties and density. The characterized properties of sample 1 will be used to obtain the real thermal conductivity of the fabricated amorphous TiO_2 nanotube. As shown in Fig. 1(b), an infrared laser beam with wavelength of 809 nm is used to periodically irradiate the sample surface, where the gold coating absorbs the laser energy and heats the layers underneath. Such laser heating will lead to a periodical temperature variation at the surface of the gold layer. This temperature variation is strongly dependent on the thermal transport in the TiO_2 nanotube arrays. In the experiment, the surface temperature variation is measured by sensing the thermal emission from the heating area using an infrared detector. The phase shift ($\Delta\phi$) of the surface temperature variation is measured over a frequency (f) range. This frequency range is carefully selected to ensure that the thermal diffusion depth within one heating period is much smaller than the heating spot. Consequently, the heat transfer within each heating period can be treated as one dimensional along the thickness direction.[17] Then trial values of the density and thermal conductivity of the TiO_2 nanotube arrays are used to

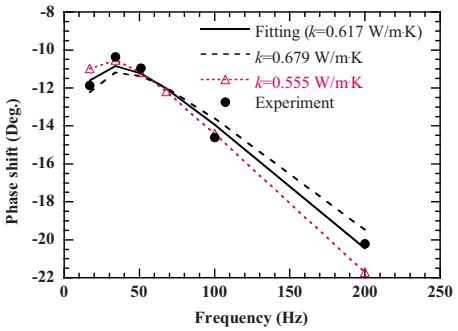

FIG. 2. (Color online) The measured phase shift of surface temperature variation in the PT experiment vs the fitting results for the TiO_2 nanotube arrays (sample 1: 29.2 μm thick). Also shown in the figure are the fitting curves using different thermal conductivity values to demonstrate experimental uncertainty.

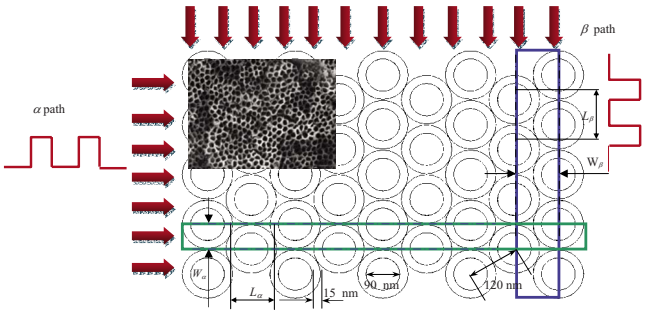

FIG. 3. (Color online) Schematic of the heat flow direction along the cross tube direction. The inset is the SEM image of the top view of TiO_2 nanotube arrays from work done by Wang and Lin (Ref. 1). L_α and L_β are the calculation units in α and β paths. W_α and W_β are the width of the two paths.

fit the measured $\Delta\phi \sim f$ curve. The trial values giving the best fit (least square) of the experimental data are taken as the properties of the material. More details about the PT technique, including experimental setup and system calibration can be found in another work by our group.[17] In our PT measurement, the laser heating spot on the sample surface is about 0.7×1.4 mm^2.

To fit the density and thermal conductivity of the as-prepared TiO_2 nanotube arrays in the PT experiment, its specific heat (c_p) is needed. Dames *et al.*[21] found that the specific heat of TiO_2 nanotubes approaches the bulk value as temperature increased from 1 to 100 K. So assuming that the specific heat of TiO_2 nanotube arrays is close to the bulk value at the experiment temperature (room temperature), from experimental results by Martan *et al.*[22] (volume-based specific heat capacity of bulk amorphous TiO_2: 2.84×10^6 J m^{-3} K^{-1}) and Lee and Cahill[23] (density of amorphous TiO_2, ρ_{bulk}: 3.9 g/cm^3), the specific heat of amorphous TiO_2 nanotube is calculated as 7.28 J kg^{-1} K^{-1} and is used in our data processing. From the Handbook of Mineralogy,[24] the specific heat and density of anatase TiO_2 are found as 688.6 J/kg K and 3.89 g/cm^3, respectively.

III. RESULTS AND DISCUSSION

A. Thermal transport along the axial direction of amorphous TiO_2 nanotubes

The experimental result and the fitting curve for the phase shift is shown in Fig. 2. The fitted density and thermal conductivity are 0.631 g/cm^3 and 0.617 W K^{-1} m^{-1}, respectively. Also shown in Fig. 2 are two theoretical curves using different thermal conductivity values while the density is fixed at 0.631 g/cm^3 to show the experimental uncertainty. It is observed that the fitted thermal conductivity has an uncertainty of 10%. The same uncertainty is found for the fitted density as well. As illustrated in Fig. 1, there is a thin layer of TiO_2 nanowires on the top of the TiO_2 nanotube array. The thickness of this layer is about 100–200 nm based on SEM observation. The overall thickness of the TiO_2 nanotube array is about 30 μm and the overall thermal resistance of the TiO_2 nanotube array is about 4.86×10^{-5} K m^2 W^{-1}. Even if we assume a much smaller thermal conductivity (e.g., 0.1 W K^{-1} m^{-1}) for the TiO_2 nanowire layer, its thermal resistance is only about $(1-2) \times 10^{-8}$ K m^2 W^{-1}, which is much smaller than that of the TiO_2 nanotube array. As for the thermal contact resistance between the TiO_2 nanowire layer and the TiO_2 nanotube array, our comprehensive investigation of the theoretical fitting does not reveal significant value.

The thermal conductivity measured here is in fact an effective value that includes the effect of the spacing between and within the nanotubes. The real thermal conductivity of the material can be found by considering the porosity of the TiO_2 nanotube arrays. According to the model proposed by Zhu *et al.*,[7] the theoretical porosity of the as-prepared sample is 60% based on the structure shown in Fig. 3. This theoretical prediction is calculated using inner pore diameter, average wall thickness, and center-to-center pore distance of 90, 15, and 120 nm, respectively. However, based on the measured density using our PT technique (0.631 g/cm^3), the porosity of the TiO_2 nanotube array is found as $(1-\rho_{eff}/\rho_{bulk})=83.8\%$. The difference between the two values indicates high porosity/spacing among/within nanotubes. The above theoretical porosity (60%) is based on an ideal structure, as shown in Fig. 3. For real TiO_2 nanotube arrays, the nanotubes cannot be that highly compacted. This will make the porosity level higher. SEM images of TiO_2 nanotube arrays in literatures[3,7,8] showed that the average pole distance is larger than the tube outside diameter, indicating loose contact among nanotubes. Additionally, defects in the nanotubes will also give contribution to the reduced density reported in this work. Based on our measured density, the real thermal conductivity (k) of TiO_2 nanotubes in this work is calculated as $k=k_\parallel/(\rho_{eff}/\rho_{bulk})=3.82$ W K^{-1} m^{-1}. This real thermal conductivity calculation is physically reasonable considering the fact that our measured effective thermal conductivity $k_\parallel$ is for heat transfer along the tube axial direction. Highly ordered orientation exists in this direction, as shown in Fig. 1(a). Since there are few references available to compare with for the thermal properties of TiO_2 nanotube arrays, our result is compared with the work done on amorphous TiO_2 thin films by Cahill and Allen.[15] In their work, the thermal conductivity at 300 K increased from 1.0 to 1.6 W K^{-1} m^{-1} as the porosity decreased from $12 \pm 3\%$ to $4 \pm 3\%$. The lower thermal conductivity in their work is probably due to the existence of nanopores in the film.

B. Thermal transport in the cross-tube direction of amorphous TiO_2 nanotubes

As discussed above, although there is no thermal contact resistance along the tube axial direction, it does exist in the cross-tube direction between the tubes. This may lead to the reduction of effective thermal conductivity in the cross-tube direction and cause the material to appear anisotropic. To investigate the thermal conductivity in the cross-tube direction, the TET technique developed in our group by Guo *et al.*[16] is employed to measure sample 2, which is comprised of highly ordered freestanding TiO_2 nanotubes (140 μm long), as shown in Fig. 1(c). The TET technique overcomes the drawbacks of the 3ω (Ref. 15) method and optical-heating-electrical-thermal-sensing technique,[25] and is capable of conducting the thermal diffusivity measurement for micro/nanoscale wires/tubes with significantly reduced experiment time and highly improved measurement accuracy.[16] In this technique, the sample is suspended between two electrodes. A square wave ac current [as shown in Fig. 1(c)] is applied to the sample to induce a periodical electric heating. The electrical resistance of the sample is 3.188 Ω for sample 2(a) and 1.842 for sample 2(b). The temperature evolution of the sample is tightly related to the heat transfer along the sample. And it will cause a variation of the electric resistance of the sample. By measuring variation of the voltage over the sample, the temperature evolution of the sample can be sensed. Consequently, the thermal diffusivity of the sample can be obtained by fitting the temperature change curve against time. Because TiO_2 nanotube is a semiconducting material, a thin layer of gold has to be deposited on the surface to make it electrically conductive. The coated layer is thin enough comparing to the thickness of the sample. Thus the thermal effect caused by the coated layer can be subtracted by using the Lorenz number without increasing the uncertainty.[16] The thermal diffusivity (α) of sample 2 is calculated by Eq. (1) as[16]

$$\alpha = \alpha_e - \frac{L_{\text{Lorenz}} TL}{RA_w \rho_{\text{eff}} c_p}, \tag{1}$$

where α_e is the measured thermal diffusivity, L_{Lorenz} ($=2.36\times10^{-8}$ W Ω K^{-2}) is the Lorenz number for Au at 300 K, T is room temperature (300 K), L is the sample length, R is the measured resistance of the sample, and A_w is the cross-sectional area of the sample, which is calculated as 140 $\mu\text{m}\times W$, where W is width of the sample.

Before the experiment is conducted, the TiO_2 nanotube arrays for sample 2 are removed from the Ti substrate by mild ultrasonication [Fig. 1(c)]. According to the SEM characterization, very limited damage to the nanotube arrays was induced during the process of the detachment from the Ti substrate. This is because the barrier layer between the nanotube arrays and Ti substrate is relatively weak and can be easily broken during mild ultrasonication.[20] The bottom of nanotube arrays was found to be closed after ultrasonication (Fig. 4) and showed no damage. Unlike the PT experiment, only a small piece is needed in the TET experiment. Figure 5 shows the pictures of two tested samples cut off from sample 2 and connected between two electrodes. Sample 2(a) has a

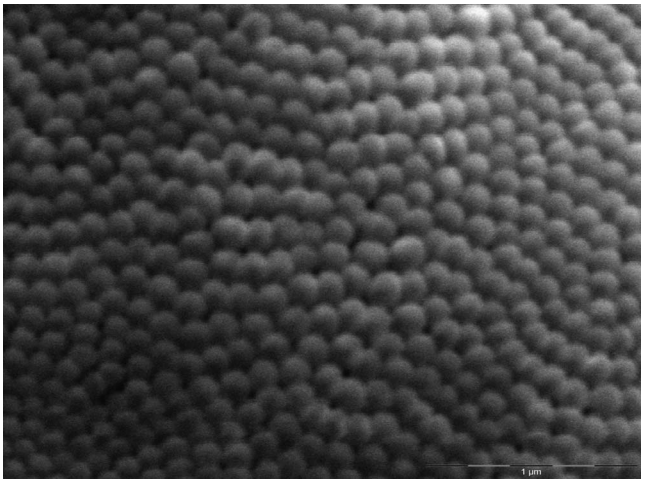

FIG. 4. SEM image of the bottom of the TiO_2 nanotube arrays. The closed end of nanotube bottoms is clearly evident.

dimension about 1.132×0.693 mm^2 and sample 2(b) 1.470×0.615 mm^2. Sample 2(a) is coated with a 260 nm thick Au film on the tube bottom side, and sample 2(b) is coated with a 200 nm thick Au film on both the tube bottom side and the surface of the nanowires layer. After coating, each sample is suspended between two copper electrodes and glued with silver paste.

The normalized temperature increase against time and the theoretical fittings for sample 2(a) and sample 2(b) are shown in Fig. 5. For sample 2(a), the effective thermal diffusivity is found to be 2.23×10^{-7} m^2/s. Based on the density measured from the PT experiment and specific heat mentioned above, the effective thermal conductivity ($k_\perp$) of the amorphous TiO_2 nanotube arrays in the cross tube direction is calculated as 0.102 W K^{-1} m^{-1}. For sample 2(b), the effective thermal diffusivity and $k_\perp$ are 1.67×10^{-7} m^2/s and 0.077 W K^{-1} m^{-1}, respectively. These values are significantly smaller than the one in the length direction (0.617 W K^{-1} m^{-1}). Since the TiO_2 is amorphous in this work, for the tube wall itself, the thermal conductivity is expected to be isotropic. The anisotropic effective thermal conductivity of the TiO_2 nanotube arrays is due to the anisotropic structure of the array itself. Based on the measured $k_\perp$,

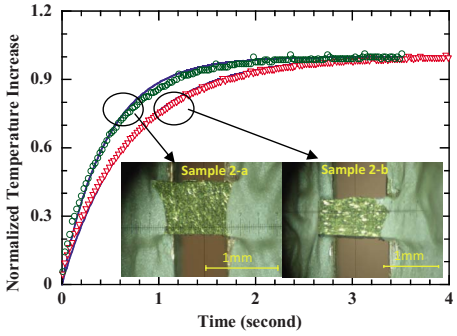

FIG. 5. (Color online) Normalized temperature increase vs the fitting results for the TiO_2 nanotube arrays in the cross tube direction, measured by TET experiments. The solid lines are the theoretical values for each sample. The circles are the experimental data measured for sample 2(a) and the triangles are the experimental data for sample 2(b). The insets are the sample pictures under microscope.

one very important property: the thermal contact resistance (R_{tc}) between the TiO_2 nanotubes can be calculated.

C. Evaluation of thermal contact resistance among amorphous TiO_2 nanotubes

For the tube array structure shown in Fig. 3, we choose two main paths: α and β for the thermal contact resistance analysis since the real heat transfer direction in the TET experiment is not exactly known. From the effective thermal resistance (R_{eff}) and the thermal resistance along the tube wall (R), the thermal contact resistance between the tubes along the two paths can be expressed as

$$R_{tc,\alpha} = R_{eff,\alpha}/N_\alpha - 2R, \tag{2}$$

$$R_{tc,\beta} = 1.5R_{eff,\beta}/N_\beta - 2R, \tag{3}$$

where $R_{eff}=L/(k_\perp hW)$ is the effective thermal resistance of a selected region shown in Fig. 3 with h the array thickness, $W=W_\alpha$ or W_β is the sample width shown in Fig. 3. $R_{eff,\alpha}$ and $R_{eff,\beta}$ are calculated from the measured thermal conductivity of the TiO_2 nanotube arrays with respect to different path width, R is the heat transfer resistance along the tube wall in the cross tube direction for 60°: $R=r_0\pi/(3kh\delta r)$ with r_0 the midpoint radius of the tube wall and δr the wall thickness, R_{tc} is the contact resistance between two tubes, and $N_\alpha(=L/L_\alpha)$ and $N_\beta(=L/L_\beta)$ are the numbers of the calculation unit in the two paths. The calculation shows that the thermal contact resistance between two nanotubes of unit length has the same value using the both path analysis, which is 15.1 for sample 2(a) and 20.6 K m^2 W^{-1} for sample 2(b). The difference between the two values may come from the experimental uncertainty and the structure variation. The side view of TiO_2 nanotube arrays in Fig. 1(a) shows that the structures from different part of the sample may vary due to the interior defect. In our TET experiment, it is found that the sample is very easy to break when it is connected between two electrodes. This is largely due to the loose contact between TiO_2 nanotubes. Longer (in cross tube direction) samples are easier to break due to the large stretching force inside induced by connection. This stretching force makes the contact worse among nanotubes and gives rise to the lower thermal diffusivity (higher thermal contact resistance) for sample 2(b) in comparison with sample 2(a). The measured thermal contact resistance reflects the capability of heat conduction between TiO_2 nanotubes. The real contact area between two adjacent nanotubes is difficult to evaluate. For two TiO_2 nanotubes of unit length, if they have a contact area in the order of 10^{-8} m^2 (meaning ~10 nm contact line between the two nanotubes), the measured thermal contact resistance gives a classical thermal contact resistance in the order of 10^{-7} K m^2 W^{-1}.

In the above thermal contact resistance analysis, the evaluation is based on ideally highly packed nanotubes. As we discussed in the PT experimental results, the density of the nanotube array is less than that of ideally packed arrays. If we assume that the ratio of real density of the nanotube array over that of ideally packed ones is γ, under such situations, in Eqs. (2) and (3), the unit width for analysis: W_α *or* W_β will be enlarged by $\sqrt{\gamma}$. At the same time, since the nanotubes are looser than the ideal situation, their separation will be enlarged by $\sqrt{\gamma}$ as well. As a result, the number of nanotubes: N_α or N_β within the unit length of consideration (Fig. 3) will be reduced by a factor of $\sqrt{\gamma}$. In Eqs. (2) and (3), the terms $R_{eff,\alpha}/N_\alpha$ and $R_{eff,\beta}/N_\beta$ have the denominator of $W_\alpha N_\alpha$ or $W_\beta N_\beta$. It is readily to prove that nonideally packed situation will not alter the thermal contact resistance obtained above.

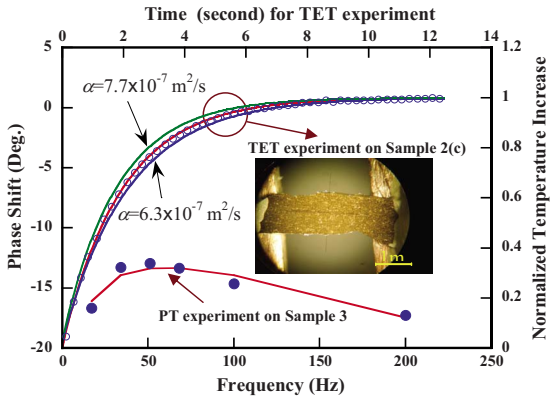

FIG. 6. (Color online) Phase shift and fitted curve vs frequency for PT experiment (sample 3, 30.7 μm) (lower left axis); normalized temperature increase and the fitting results vs time for the TiO_2 nanotube arrays in the cross tube direction [sample 2(c), 140 μm] (upper right axis), measured by the TET experiments. The solid lines are the theoretical values for each sample. The circles and dots are the experimental data measured for each sample. The inset is the picture of sample 2(c) under microscope. Also shown in the figure are the fitting curves for the TET experiment using different thermal diffusivity values to demonstrate the experimental uncertainty.

D. Anisotropic thermal transport in anatase TiO_2 nanotubes

The PT and TET experiments are also conducted on anatase TiO_2 nanotube arrays to study the anisotropic thermal transport in them. For the PT experiment, sample 3 is used, which is about 30.7 μm thick and coated with a 200 nm gold coating on top of the nanowire layer. For the TET experiment, sample 2(c) measures 3.69 mm, 1.05 mm, and 140 μm in length, width, and thickness, respectively. It is coated with a 150 nm gold on both the top of the nanowire layer and the bottom of the nanotube arrays. The resistance of sample 2(c) after coating is 1.79 Ω. The experimental results and fitting curves are shown in Fig. 6. The specific heat used in the curve fitting is 688.6 J/kg K for the PT experimental results. The fitted thermal conductivity is 1.12 W K^{-1} m^{-1} ($k_\parallel$) in tube length direction. In the cross tube direction by the TET measurement, the effective thermal diffusivity is 7.00×10^{-7} m^2/s. The real thermal diffusivity of the sample excluding the effect of the gold coating is 4.97×10^{-7} m^2/s and corresponding thermal conductivity ($k_\perp$) is 0.24 W K^{-1} m^{-1} in the cross tube direction. This result indicates strong anisotropic thermal conductivity in the anatase TiO_2 nanotube arrays. Compared with the amorphous TiO_2 nanotube arrays measured above, the anatase

TiO_2 nanotube arrays have a much higher thermal conductivity, about two times the values of amorphous TiO_2 nanotube arrays.

Also shown in Fig. 6 are the theoretical curves for the TET experiment using two different thermal diffusivities: 7.7×10^{-7} and 6.3×10^{-7} m^2/s. It is found that the TET experiment has an uncertainty of 10% when characterizing the thermal diffusivity. Such uncertainty also holds on for the measurement of samples 2(a) and 2(b) illustrated in Fig. 5. In the TET experiment, the characteristic time (t_1) of heat transfer (along the axial direction of the tube) in the cross-sectional direction of the sample is about 3.95×10^{-4} s ($\sim\delta/\alpha_{\parallel}^2$: δ, thickness of the sample; $\alpha_{\parallel}$, thermal diffusivity in the nanotube axial direction). On the other hand, along the sample length direction, the characteristic heat transfer time (t_2) is about 19 s ($\sim l/\alpha_{\perp}^2$: l, length of the sample; $\alpha_{\perp}$, effective thermal diffusivity in the cross tube direction). Therefore during the TET experiment, the heat transfer in the cross-sectional direction of the sample is significantly faster than that in the length direction, which makes it safe to assume the sample has uniform temperature distribution in its cross section. It is physically reasonable to assume that the heat transfer is one-dimensional along the length (3.69 mm) direction of the sample.

As discussed above, the fitted thermal conductivity $k_{\parallel}$ contains the porosity effect, which can be estimated using ratio of the fitted density and the bulk density. So the real thermal conductivity of sample 2(c) can be estimated by $k=k_{\parallel}/(\rho_{\mathrm{eff}}/\rho_{\mathrm{bulk}})=6.12$ W K^{-1} m^{-1}, where the fitted effective density and the bulk anatase density is 0.713 and 3.89 g/cm^3, respectively. It is noted that the effective density of the anatase TiO_2 nanotube arrays is fitted to be 0.713 g/cm^3, which is quite close to the result for the amorphous TiO_2 nanotube arrays: 0.631 g/cm^3. This shows that after annealing to become anatase phase, the TiO_2 nanotube array has little change in the overall array structure. Its real thermal conductivity (6.12 W K^{-1} m^{-1}) is a little smaller than that of bulk anatase TiO_2 (8.5 W K^{-1} m^{-1}).[24] Maekawa *et al.*[26] measured the thermal conductivity of anatase TiO_2 thin films of different structures and the results are 5.1–6.7 W K^{-1} m^{-1} for dense structures and 0.24 W K^{-1} m^{-1} for feather like structures in the in-plane direction. They believe the lower thermal conductivity for dense structure is due to the reduced density compared to bulk material. For the feather like structures, they explained that the extremely low thermal conductivity is probably due to the structure perpendicular to the heat flow direction that barred the heat flow, which is quite similar to the heat transfer in the cross tube direction in this work. Using Eqs. (2) and (3), the unit length thermal contact resistance is calculated as 5.90 K m^2 W^{-1} for the anatase TiO_2 nanotube arrays. This number is much smaller than that for the amorphous TiO_2 nanotubes measured above, indicating better thermal contact between anatase TiO_2 nanotubes.

IV. CONCLUSION

In conclusion, the thermal conductivity of TiO_2 nanotube arrays in both the tube length and cross-tube directions was measured for the first time. Strong anisotropic effective thermal conductivity was observed in our work: 0.617 W K^{-1} m^{-1} along the tube length direction and 0.077–0.102 W K^{-1} m^{-1} in the cross tube direction for amorphous TiO_2 nanotube arrays. For anatase TiO_2 nanotube arrays, their thermal conductivity is much higher than that of the amorphous ones: 1.12 W K^{-1} m^{-1} in the axial direction and 0.24 W K^{-1} m^{-1} in the cross tube direction. Using the PT technique, the density of TiO_2 nanotube arrays was also characterized. Although from the top view of the TiO_2 nanotube arrays, the density of the as-prepared sample was geometrically estimated as 1.56 g/cm^3, the actual density is much lower (0.639 g/cm^3 for amorphous and 0.713 g/cm^3 for anatase) due to the loose contact between tubes and defects in nanotubes. The thermal contact resistance between TiO_2 nanotubes was characterized by utilizing both the PT method and TET technique. For amorphous TiO_2 nanotubes, the unit length thermal contact resistance was 15.1 and 20.6 K m^2 W^{-1} for the two measured samples, while a lower thermal contact resistance of 5.90 K m^2 W^{-1} was obtained for the anatase TiO_2 nanotubes.

ACKNOWLEDGMENT

Support of this work from NSF (Grant No. CBET 0931290) and start-up fund of Iowa State University is gratefully acknowledged.

[1] J. Wang and Z. Q. Lin, Chem. Mater. **20**, 1257 (2008).
[2] J. M. Perez-Blanco and G. D. Barber, Sol. Energy Mater. Sol. Cells **92**, 997 (2008).
[3] J. Park, S. Bauer, K. V. D. Mark, and P. Schmuki, Nano Lett. **7**, 1686 (2007).
[4] V. M. Prida, E. Manova, M. Hernandex-Velez, P. Aranda, K. R. Pirota, M. Vazquez, and E. Ruiz-Hitzky, J. Magn. Magn. Mater. **316**, 110 (2007).
[5] M. Paulose, H. E. Prakasam, O. K. Varghese, L. Peng, K. C. Popat, G. K. Mor, T. A. Desai, and C. A. Grimes, J. Phys. Chem. C **111**, 14992 (2007).
[6] J. Park, S. Kim, and A. J. Bard, Nano Lett. **6**, 24 (2006).
[7] K. Zhu, N. R. Neale, A. Miedaner, and A. J. Frank, Nano Lett. **7**, 69 (2007).
[8] O. K. Varghese, D. Gong, M. Paulose, K. G. Ong, and C. A. Grimes, Sens. Actuators B **93**, 338 (2003).
[9] P. Xiao, D. Liu, B. B. Garcia, S. Sepehri, Y. Zhang, and G. Cao, Sens. Actuators B **134**, 367 (2008).
[10] J. A. Toledo-Antonio, S. Capula, M. A. Corts-Jcome, C. Angeles-Chvez, E. Lopez-Salinas, G. Ferrat, J. Navarrete, and J. Escobar, J. Phys. Chem. C **111**, 10799 (2007).
[11] G. K. Mor, K. Shankar, M. Paulose, O. K. Varghese, and C. A. Grimes, Nano Lett. **6**, 215 (2006).
[12] S. Funk, B. Hokkanen, U. Burghaus, A. Ghicov, and P. Schmuki, Nano Lett. **7**, 1091 (2007).
[13] S. Oh, C. Daraio, L. Chen, T. R. Pisanic, R. R. Fiñones, and S. Jin, J. Biomed. Mater. Res. Part A **78**, 97 (2006).
[14] S. P. Albu, A. Ghicov, J. M. Macak, R. Hahn, and P. Schmuki, Nano Lett. **7**, 1286 (2007).
[15] D. G. Cahill and T. H. Allen, Appl. Phys. Lett. **65**, 309 (1994).
[16] J. Guo, X. Wang, and T. Wang, J. Appl. Phys. **101**, 063537 (2007).
[17] T. Wang, X. Wang, Y. Zhang, L. Liu, L. Xu, Y. Liu, L. Zhang, Z. Luo, and K. Cen, J. Appl. Phys. **104**, 013528 (2008).
[18] J. Wang and Z. Lin, J. Phys. Chem. C **113**, 4026 (2009).
[19] M. Paulose, K. Shankar, S. Yoriya, H. E. Prakasam, O. K. Varghese, G. K. Mor, T. A. Latempa, A. Fitzgerald, and C. A. Grimes, J. Phys. Chem. B **110**, 16179 (2006).
[20] J. Wang, L. Zhao, V. S. Y. Lin, and Z. Lin, J. Mater. Chem. **19**, 3682 (2009).
[21] C. Dames, B. Poudel, W. Z. Wang, J. Y. Huang, Z. F. Ren, Y. Sun, J. I. Oh, C. Opeil, M. J. Naughton, and G. Chen, Appl. Phys. Lett. **87**, 031901 (2005).

[22]J. Martan, O. Herve, and V. Lang, J. Appl. Phys. **102**, 064903 (2007).
[23]S. M. Lee and D. G. Cahill, Phys. Rev. B **52**, 253 (1995).
[24]J. W. Anthony, R. A. Bideaux, K. W. Bladh, and M. C. Nichols, *Handbook of Mineralogy Volume III Halides, Hydroxides, Oxides* (Mineral Data Publishing, Arizona, 1997).
[25]J. Hou, X. Wang, and J. Guo, J. Phys. D: Appl. Phys. **39**, 3362 (2006).
[26]T. Maekawa, K. Kurosaki, T. Tanaka, and S. Yamanaka, Surf. Coat. Technol. **202**, 3067 (2008).